Strain-based methodology for mixed-mode I+II fracture: a new partitioning method for bi-material adhesively bonded joints

Marcio Moreira Arouche[a,b*], Wandong Wang[b], Sofia Teixeira de Freitas[b], Silvio de Barros[a,c]

[a]Laboratory of Composites and Adhesives, Federal Centre for Technological Education of Rio de Janeiro, Rio de Janeiro, Brazil;

[b]Structural Integrity & Composites Group, Faculty of Aerospace Engineering, Delft University of Technology, Delft, The Netherlands;

[c]Institut de Recherche en Génie Civil et Mécanique, Université de Nantes, Saint-Nazaire, France

*corresponding author: marcio.m.arouche@gmail.com

Abstract

The dissemination of composite materials introduces applications of hybrid structures with composite and metal parts. The development of reliable methodologies to evaluate the performance of these structures is required. In this work, the mixed-mode fracture behaviour of a bi-material adhesively bonded joint is investigated. A new strain-based criterion for the design of the Mixed-Mode Bending (MMB) bi-material specimen is suggested. A new analytical partitioning method based on the 'global method' is proposed and tested on a composite-to-metal bonded joint and compared with a finite element model using the virtual crack closure technique (VCCT). The results show that the proposed strain-based design methodology can be successfully used in MMB test for bi-material joints. The fracture mode partitioning is accurately predicted by the analytical method. However, the absolute values of the strain energy release rate (SERR) predicted by the analytical method are only accurate if the shear deformation in the test is not significant.

Keywords: fracture mechanics, analytical models, finite element analysis, composites, mixed-mode fracture, MMB test

1. Introduction

In recent years, composite materials have become widely used in structural applications. This technology has been developed in aerospace industry [1] and disseminated to numerous fields, such as automotive [2], marine [3] and construction [4]. Fibre-reinforced polymers (FRPs) are most commonly applied due to their high strength-to-weight ratio. The dissemination of these materials introduces applications of hybrid structures with composite and metal parts [5]. Adhesive bonding is the most efficient technology in terms of weight and performance to join these two materials. The advent of composite-to-metal bonded joints requires the development of reliable methodologies to evaluate the performance of these structures [6-8].

Fracture mechanics is an important instrument to improve the design and performance of adhesively bonded structures. Imperfections present within materials are points of stress concentration and therefore fracture initiation. Fracture mechanics models the defect as a crack and evaluates if its size overcome the critical fracture size leading to structural failure. The strain energy release rate (SERR) is the most important property to consider in the calculation of fracture toughness of cracked structures. The crack propagation occurs when the available energy at the crack tip (G) exceeds the critical energy for crack propagation (G_c) [9]. In-service structures are commonly subjected to a combination of peeling and shear stresses. This means that a combination of modes I and II loadings occurs at the crack tip.

A variety of mixed-mode fracture test methods has been developed for evaluation of the mixed-mode (I+II) fracture toughness. The Crack lap shear (CLS) test [10] has been widely used for characterization of the fracture toughness of adhesively bonded joints. The asymmetric double cantilever beam (ADCB) test [11] was suggested from a generalization of

the DCB test using a specimen with asymmetric arms. The single-leg bending (SLB) test [12] has proposed as a three-point bending test with one extremity supported only by the specimen upper arm. However, these test methods have a limited range of mode-mixities with small contribution of mode II. Different mixed mode ratios can only be obtained by changing the thickness ratios of the upper and lower arms, which requires the manufacture of specimens with different geometries.

Several mixed-mode fracture test methods have been proposed for the characterization of a wide range of mode-mixities [13-18]. Some of these works are adaptations of pure mode test methods [13-15]. Other authors developed testing jigs that induce a combination of opening and shear loadings to the specimen [16-18]. Among them, the Mix-Mode Bending (MMB) test [17] stands out for its easy implementation, reliability and capability of testing a wide range of mode-mixities with only one specimen geometry.

The MMB test method was originally developed for evaluation of delamination in unidirectional composites [19-20]. A number of authors evaluated symmetric and asymmetric delamination of multidirectional composites [21-23]. A recent work addressed the fracture toughness in dissimilar composite bonded joints [24]. Few works addressed mixed-mode fracture of metal bonded joints [25-27]. They show that the MMB test presented a difficulty due to extensive adherend yielding. Tests with wood bonded joints [28-30] and bone fracture [31] can also be found in the literature. However, no work is available on mixed-mode fracture of composite-to-metal bonded joints.

The linear elastic fracture behaviour of a bonded joint can be predicted using finite elements analysis. A number of formulations are available in literature for mixed-mode failure of bonded joints [32-33]. Among them, the virtual crack closure technique (VCCT) is widely applied and commonly available in most of the commercial finite elements method softwares. The VCCT is based on the assumption that the energy released when the crack is extended a

crack tip element size is identical to the energy required to close the crack in the same length. This is an accurate method for calculation of the fracture energy at the crack tip in homogenous materials [33]. However, when the crack is located in a bi-material interface, the mode partitioning become sensitive to the crack extension length [34]. One method proposed by literature to circumvent this problem is the introduction of an interlayer between the crack interface and placing the crack within it [23-24]. The crack propagation occurs within a homogeneous path where the mode partition is not sensitive to the crack length.

In this work, the mixed-mode fracture behaviour of a bi-material adhesively bonded joint is investigated. The aim is to propose and evaluate a new strain-based criterion for the design of MMB bi-material specimens and a new analytical partitioning method to characterize their fracture behavior under mixed-mode loadings. A composite-to-metal adhesively bonded joint is used as a case study to evaluate the proposed method.

2. Proposed Partitioning Method for Bi-Material Bonded Joints

The strain energy release rate of a cracked material can be defined as [35]:

$$G = \frac{1}{B}\left(\frac{dU_e}{da} - \frac{dU_s}{da}\right) \tag{1}$$

Where B is the specimen width, a is the crack length, U_e is the external work and U_s is the strain energy. The formulation for the total SERR (G) is then obtained for linear elastic material behaviour [36]:

$$G = \frac{1}{2B}\left(\frac{M_1^2}{E_1 I_1} + \frac{M_2^2}{E_2 I_2} - \frac{(M_1 + M_2)^2}{EI}\right) \tag{2}$$

Where E_1, I_1, E_2, I_2, E and I are the elastic moduli and second moments of area in the section of the crack tip of the upper arm, lower arm and beam, respectively. M_1 and M_2 are the bending moments on the section of the crack tip in the upper and lower arms, respectively. This equation is valid for a crack propagation along a defined path between two arms under bending moments, as shown in Figure 1.

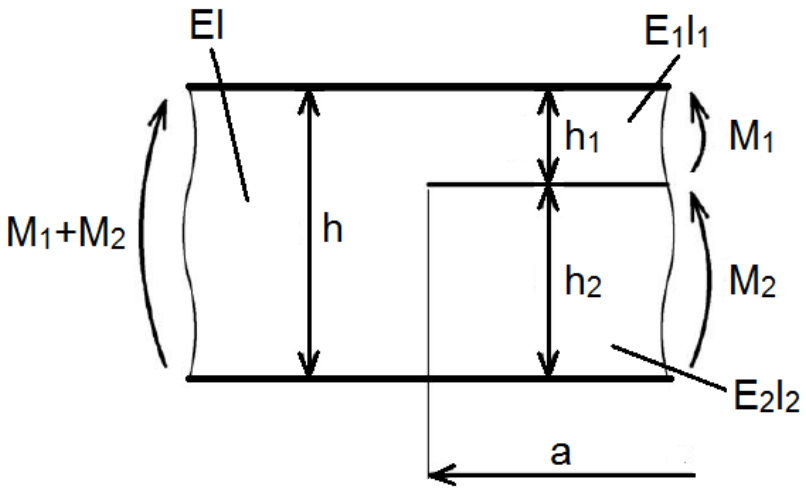

Figure 1: Crack propagation parameters.

Regarding the MMB test, mixed-mode fracture is induced by an opening and shear loadings applied to the specimen. A schematic of the MMB test set-up is shown in Figure 2.

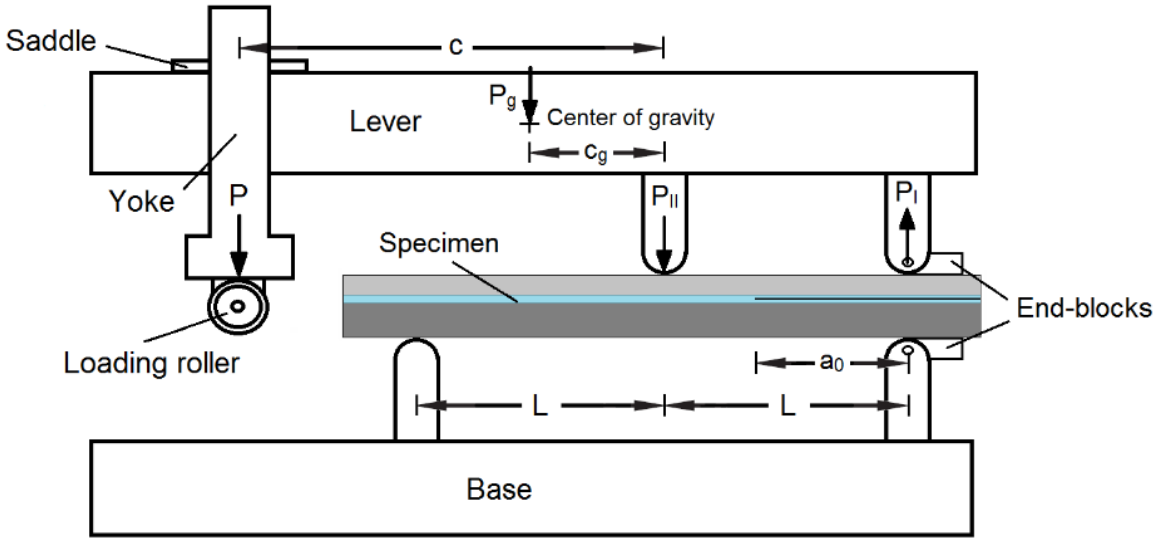

Figure 2: Schematic of the MMB test.

The resulting bending moments are:

$$M_1 = \frac{Pc + P_g c_g}{L} a \tag{3}$$

$$M_2 = \frac{P(L-c) + P_g(L-c_g)}{2L} a \tag{4}$$

Where the parameters are defined in Figure 2.

The SERR of a MMB test can be obtained by replacing (3) and (4) in equation (2). This equation gives the total SERR but it is essential to distinguish the contribution of mode I and mode II fracture in order to characterize the mixed mode fracture behaviour of the joint.

Literature suggests different methods for the partitioning of mixed-mode fracture [37]. The so-called ‘global method’ [35] was one of the earliest analytical methods that successfully identified the pure modes fracture and mixed-mode partition of specimens under bending moments. It is based on the following two assumptions for the partitioning:

(i) pure mode I exists when opposite moments act on the joint arms, i.e. $M_1 = M_I$ and $M_2 = -M_I$;

(ii) pure mode II is obtained when the curvature in the two arms are the same, i.e. $M_1 = M_{II}$ and $M_2 = \psi M_{II}$, where ψ is defined as the bending stiffness ratio of upper and lower arms, as:

$$\psi = \frac{E_2 I_2}{E_1 I_1} \tag{5}$$

Based on these two assumptions, one can obtain:

$$M_1 = M_{II} + M_I \tag{6}$$

$$M_2 = \psi M_{II} - M_I \tag{7}$$

Substituting (6) and (7) in (2), the SERR can be partitioned in mode I, when $M_{II} = 0$, and mode II, when $M_I = 0$. G_I and G_{II} are then given by:

$$G_I = \frac{\left(\psi M_1 - M_2\right)^2}{2B\left(\psi + 1\right)^2}\left(\frac{1}{E_1 I_1} + \frac{1}{E_2 I_2}\right) \tag{8}$$

$$G_{II} = \frac{\left(M_1 + M_2\right)^2}{2B\left(\psi + 1\right)}\left(\frac{1}{E_1 I_1} - \frac{\left(\psi + 1\right)}{EI}\right) \tag{9}$$

Similar formulations for delamination of composite materials can be found in the literature [20, 24]. However, the ‘global method’ is only able to give the correct partition of

symmetric specimens and is limited on the prediction of fracture behavior in asymmetric geometries and materials [37].

A recent study [38] has proven that in the case of bi-material bonded joints, i.e., arms of different material, simply guaranteeing opposite moments, as assumed by the 'global method', i.e. $M_1 = M_I$ and $M_2 = -M_I$, is not sufficient to guarantee pure mode I and introduces a certain amount of mode II fracture. That same study proves that to assure pure mode I in bi-material bonded joints, the longitudinal strain distribution at the faying surfaces of both arms must be identical. Therefore, assumption (i) of the 'global method' is replaced by:

(i)' i.e. $M_1 = M_I$ and $M_2 = -\beta M_I$, where β is the longitudinal strain ratio of upper and lower arms, defined by:

$$\beta = \frac{E_2 h_2^2}{E_1 h_1^2} \tag{10}$$

Based on this new assumption, one can obtain:

$$M_1 = M_{II} + M_I \tag{11}$$

$$M_2 = \psi M_{II} - \beta M_I \tag{12}$$

Substituting (11) and (12) in (2), a new partition for MMB bi-materials joints is introduced. G_I^* and G_{II}^* are then given by:

$$G_I^* = \frac{\left(\psi M_1 - M_2\right)^2}{2B\left(\psi+\beta\right)^2}\left(\frac{1}{E_1 I_1} + \frac{\beta^2}{E_2 I_2} - \frac{\left(1-\beta\right)^2}{EI}\right) \tag{13}$$

$$G_{II}^* = \frac{\left(\beta M_1 + M_2\right)^2}{2B\left(\psi+\beta\right)^2}\left(\frac{\left(\psi+1\right)}{E_1 I_1} - \frac{\left(\psi+1\right)^2}{EI}\right) \tag{14}$$

The strain equivalence between arms assures pure mode I fracture while pure mode II is obtained when the curvature in the two arms are the same. Important to notice that if the strain-based design equivalence geometry is adopted for the design of the MMB specimens, i.e., the arms of bi-material bonded joint geometry are chosen such as $E_2 h_2^2 = E_1 h_1^2$ ($\beta = 1$), equations (11) and (12) reduce to (6) and (7) and equations (13) and (14) are equivalent to (8) and (9). In this study the geometry of the joint was chosen to satisfy the condition of $\beta = 1$.

3. Experimental Procedures

In order to test the proposed methodology, a test campaign has been conducted in which MMB tests were performed in composite-to-metal bonded joints.

3.1 Materials and specimens

Composite-to-metal test specimens were manufactured. A 6.35 mm thick carbon steel plate (σ_y = 250 MPa) was taken as metal adherend. Carbon fibre fabrics with a nominal area weight of 424 g/m^2 (LTC450-C10-C, DEVOLD AMT, Langevåg, Norway) were selected to make the composite adherend. Each fabric is composed of two orthogonal laminas of unidirectional fibres. An epoxy resin (PIPEFIX, Novatec, Rio de Janeiro, Brazil) was chosen as impregnation resin of the composite. The adhesive is an epoxy (NVT201E, Novatec, Rio de Janeiro, Brazil). Mechanical properties of the materials are shown in Table 1.

The manufacturer provided the adhesive elastic modulus and the composite properties were obtained from a previous work [39].

Table 1: Mechanical properties of the materials.

Material	E / E_1 (GPa)	E_2 (GPa)	G_{12} (GPa)	ν / ν_{12}
Carbon steel	200			0.27
Adhesive	2.25			
Carbon-epoxy ply	82	10	3.0	0.24

The manufacturing process tried to mimic as much as possible the application of composite patch repairs in oil and gas production platforms [40]. Surface preparation of the steel plate was achieved with grit blasting of G-40 steel grit and degreasing with acetone. An anti-friction material was applied over the steel surface to produce the pre-crack. The adhesive was then applied over the treated steel surface. One layer of glass fibre dry chopped strand mat with a density of 300 g/m^2 was applied to avoid direct contact between carbon fibres and metal. Then, the hand lay-up process started by alternating application of carbon fibre fabrics layers and the impregnation resin. Finally, a layer of peel ply was applied over the last composite ply in order to produce a smoother outer surface. The number of composite plies was determined in order to comply with the strain-based design criterion ($\beta = 1$). The final lay-up consisted of a $[0/90]_{20}$ carbon-fibre reinforced polymer (CFRP). The curing process was performed at room temperature for 2 h

A CFRP-to-steel plate was manufactured (180 x 400 mm) with total thickness (h) of 20.3±0.7 mm and cut to specimens of 180±1 mm length and 25±1 mm width (B). Measurements were obtained with a digital calliper from three different regions: 30 mm from the sides and at the half-length of the specimens. Finally, aluminium end-blocks (25x15x7

mm) were bonded to the specimens using an epoxy adhesive, producing a pre-crack length (a_0). Specimen geometry and boundary conditions are shown in Figure 3.

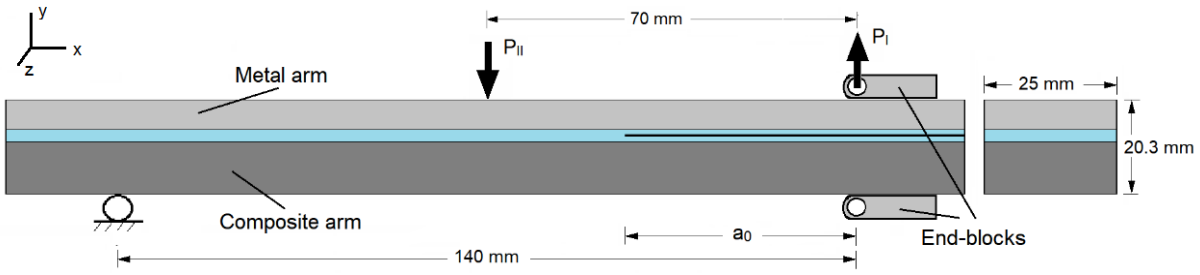

Figure 3: Specimen geometry and boundary conditions.

3.2 Test set-up

In the MMB test, a load (P) is applied by the yoke on the loading rollers attached to the lever and loaded just above the mid-plane of the test specimen. The lever applies the opening (P_I) and shear (P_{II}) loadings on the specimen in a ratio defined by the lever length (c). The contribution of shear loading increases when the lever length is reduced. A typical MMB test apparatus was used in the test - see Fig. 2 [41]. The lever weight (P_g) is 17.3 N. The test set-up was chosen to have the steel arm on top in order to avoid crack migration to the composite layers.

The side of the specimens was coated with a water-based correction fluid and millimetre paper was placed for crack length measurements. A high-resolution camera system was positioned to take photos of the crack side. Crack propagation points were acquired from the photos. Strains gauges were used in order to measure the longitudinal strain. Six strain gauges (KFG-5-120-C1-11, Kyowa Electronic Instruments, Tokyo, Japan) were glued at the free surfaces of the specimen (four on the steel adherend and two on the composite adherend).

Tests were conducted with a servo-hydraulic testing machine equipped with a 10 kN load cell. The procedure was configured for a constant displacement of 0.5 mm/min.

4. Numerical Analysis

A 3D finite elements model of the MMB test was developed in Abaqus®. Brick 8-nodes linear elements (C3D8) were applied in the whole model. Contour conditions were applied in order to simulate the real-life testing conditions. The right bottom end was constrained from all displacements and the rotations around x and y axis – see Figure 4 for coordinate system. The left bottom end was only constrained from displacements in y direction. The opening load (P_I) was applied in the right top end and the shear loading (P_{II}) was applied in the centre top surface – see Figure 3. The opening and shear loadings were obtained from Equations 3 and 4. Numerical simulations were performed according to load vs. crack length points measured from the tests. Material properties are in accordance with Table 1.

The VCCT was applied for calculation of the fracture parameters. This method is implemented as a crack propagation tool in Abaqus®. The crack propagates when the fracture energy around the crack tip exceeds a critical value. Since the simulation of the damage progression is not the aim of this study, high values of critical SERR were inserted to assure that the crack will not propagate. This allows obtaining the fracture energy at defined crack propagation points. Crack propagation was modelled within the adhesive layer, i.e., adhesive elements on both sides of the crack, as suggested in literature [23, 24].

A mesh sensitivity analysis was performed. Elements length and width (Δa) were changed in the region around the crack tip while elements height is maintained. Both sides of the crack tip have elements of the same size. Detailed mesh is shown in Figure 4. Results of the numerical analysis are shown in Figure 5. Fracture energy values are the average results obtained along crack tip. It is observed that the mode partitioning is nearly constant for elements larger than 0.25 mm around the crack tip but diverges for lower element sizes. The

results agree with stated in the literature that a larger element length is recommended for small mesh dependence [32]. The model with Δa = 0.5 mm was chosen for the determination of fracture energy with the VCCT.

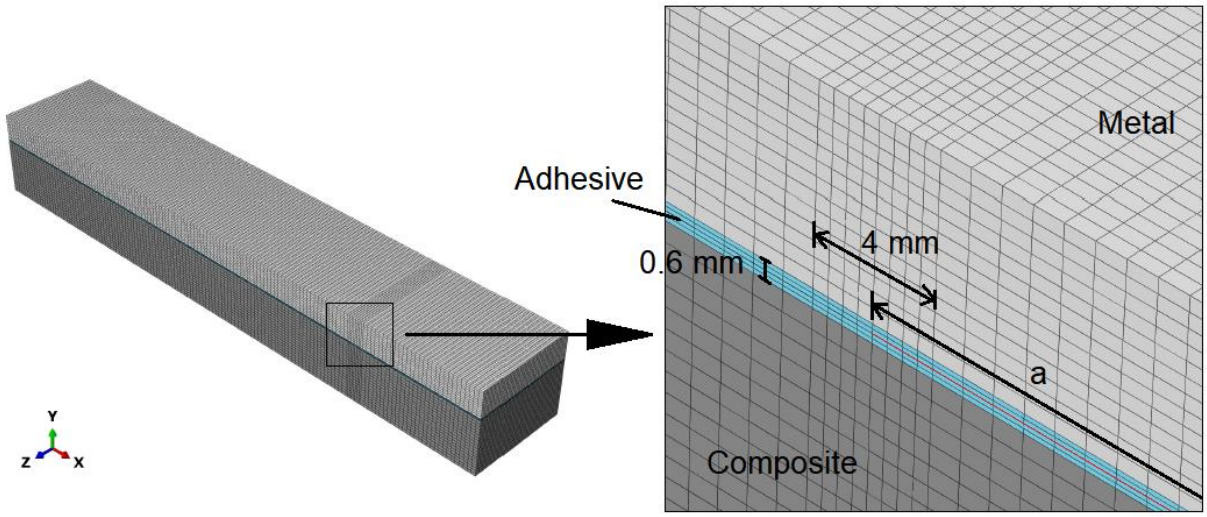

Figure 4: Finite elements mesh detail.

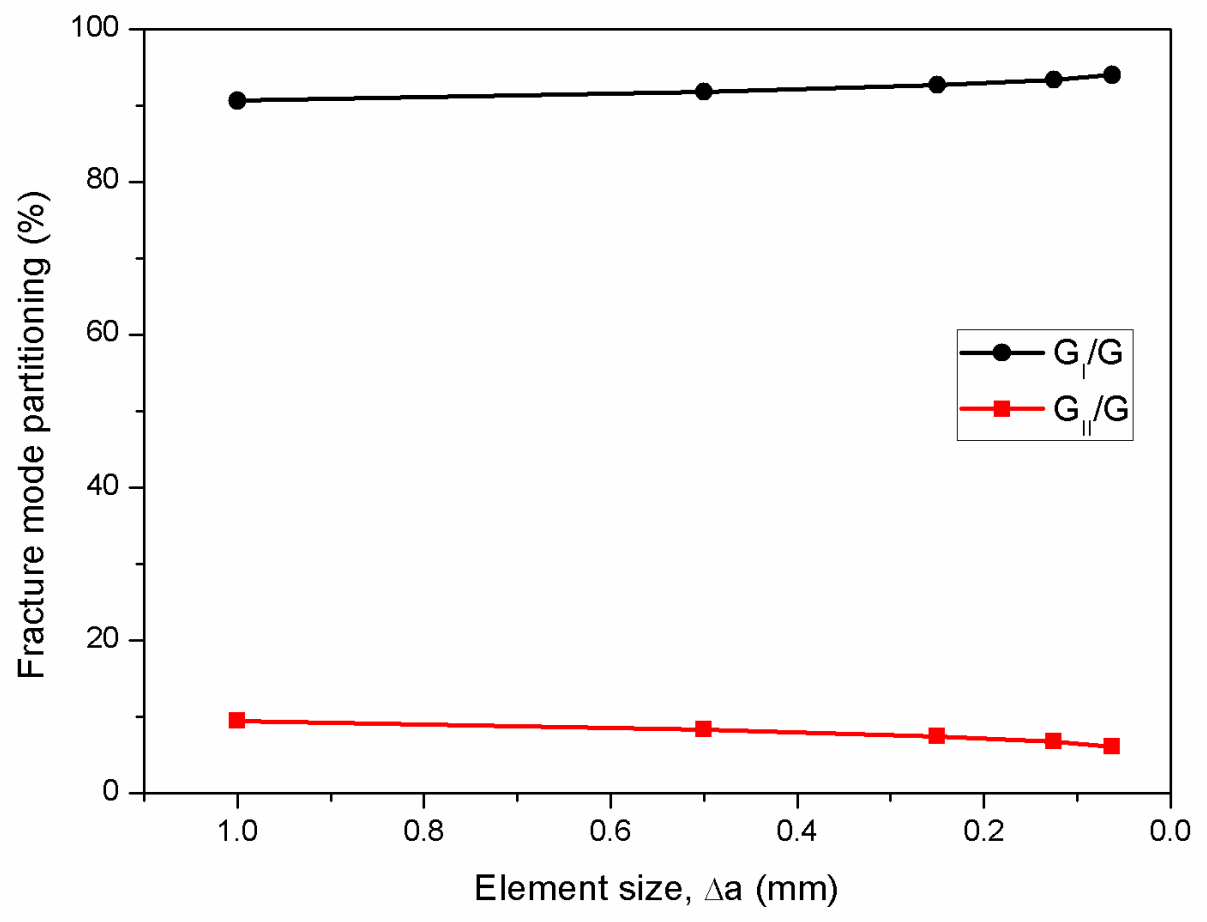

Figure 5: Finite elements mesh sensitivity.

5. Results and Discussion

5.1 Experimental results

A total of ten specimens were tested with five different test parameters. The test parameters are detailed in Table 2. The first test series, Tests 01 and 02, was performed with an initial crack of 45 mm. This initial crack was reduced to 30 mm for the remaining tests in order to increase the propagation zone. The lever length was changed between series in order to change the fracture mode ratios. Figure 6 shows the load and crack-displacement curves of each test performed, clustered for each test series. There is an acceptable scatter in the load-displacement curves of similar test parameters. Some non-linearity is perceived in the beginning of the curves due to accommodation of the test apparatus. It is observed that the test

loadings are higher when using lower lever lengths. This was expected since the reduction of the lever length decreases the mode I fracture component, and the contribution of mode I loading has a major influence in the crack propagation. Figure 7 shows images of the typical final fracture surfaces taken from an optical microscope. All tests exhibited cohesive fracture within the adhesive layer.

Table 2: Test matrix.

Test	Lever length, c (mm)	Lever centre of gravity, c_g (mm)	Initial crack, a_0 (mm)
01	104	38	45
02	104	38	45
03	104	38	30
04	104	38	30
05	78	32	30
06	78	32	30
07	64	29	30
08	64	29	30
09	50	27	30
10	50	27	30

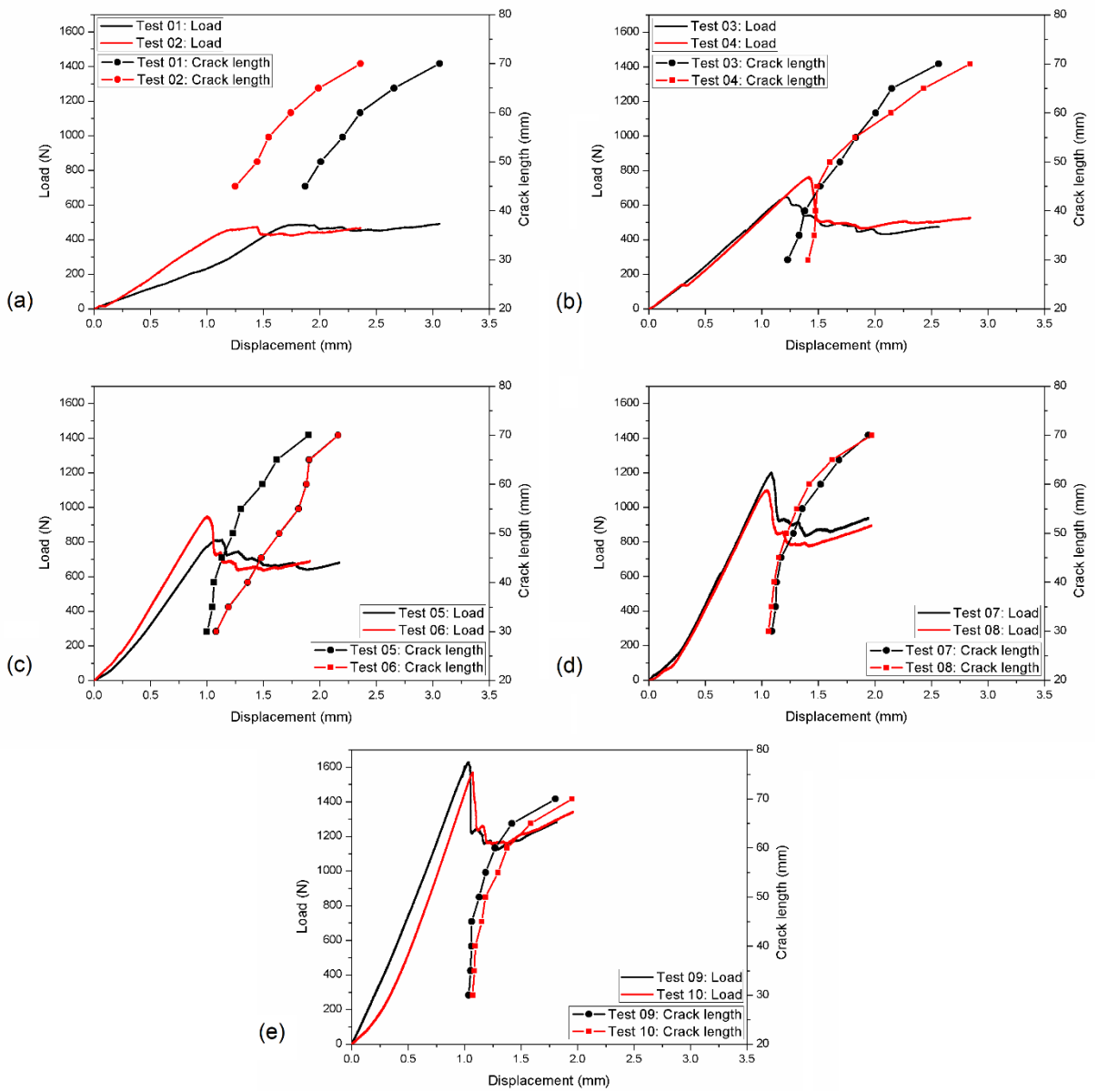

Figure 6: Load and crack length curves of Tests (a) 01 and 02, (b) 03 and 04, (c) 05 and 06, (d) 07 and 08, (e) 09 and 10.

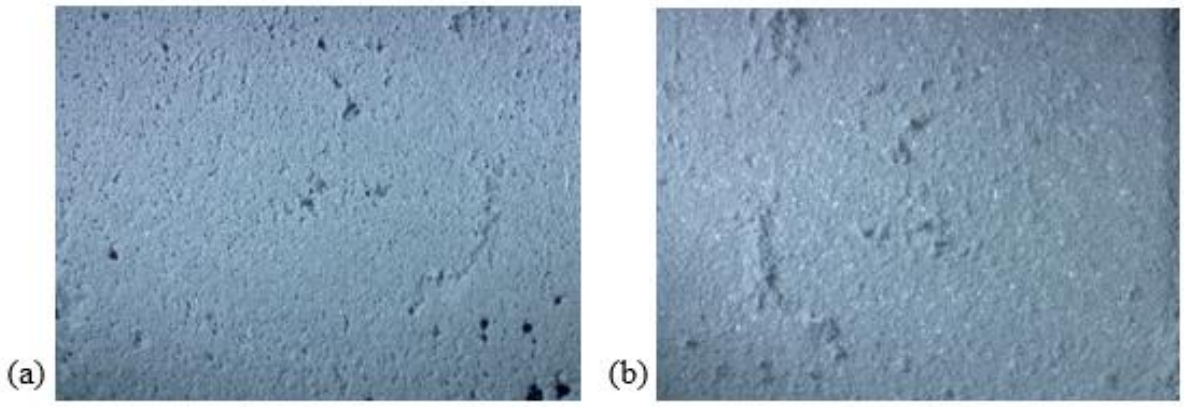

Figure 7: Fracture surfaces of (a) composite lower adherend and (b) metal upper adherend.

5.2 Validation of numerical model

For validation of the numerical model, the strains obtained from the strain gauges during experiments were compared with the FE model at loading vs. crack size specific points. Two loading cases at the crack length of 45 mm and 55 mm were considered from Test 02. The numerical strain curves were obtained along the steel and composite outer surfaces at half-width – location of the strain gauges. Figures 8 and 9 show the comparison between numerical and experimental longitudinal strain. The length axis is defined from the application point of the opening load. There is a good agreement between numerical and experimental results.

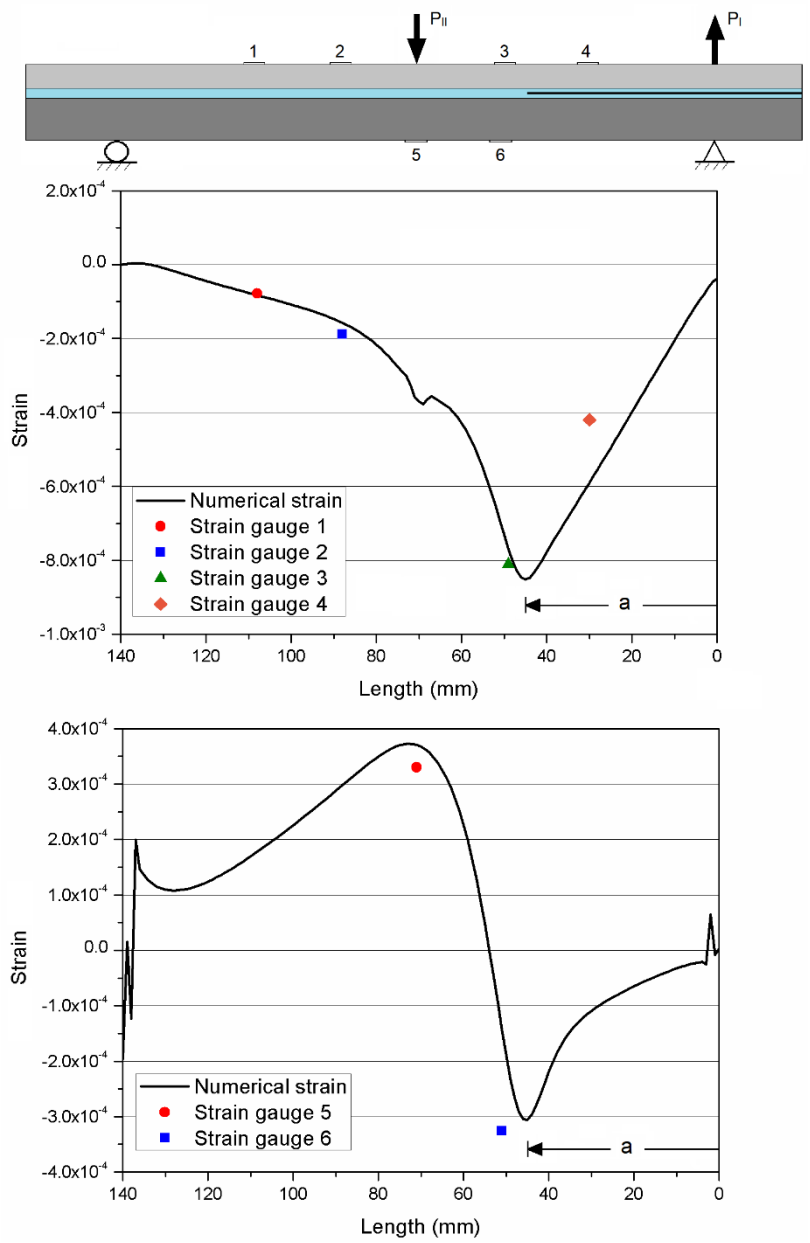

Figure 8: Test 02 strain along steel (upper graph) and composite (lower graph) surfaces at load of 456 N and crack length of 45 mm.

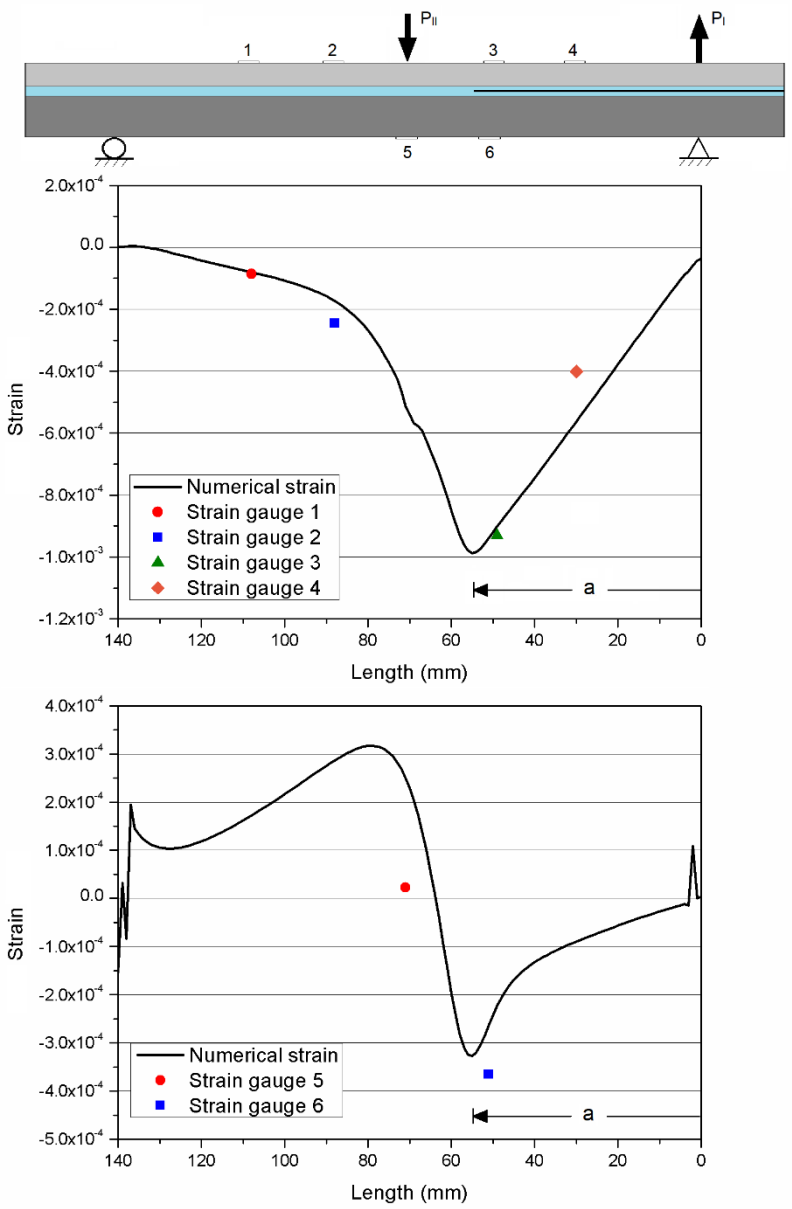

Figure 9: Test 02 strain along steel (upper graph) and composite (lower graph) surfaces at load of 432 N and crack length of 55 mm.

5.3 Fracture energy

Linear elastic condition is required for the calculation of fracture toughness. To assure that, numerical simulations were performed with experimental loading vs. crack propagation points. The maximum strain in the metal arm was obtained in every 5 mm of crack propagation. As shown in Figures 8 and 9, the region of maximum strain coincides with

the crack tip length and the strain increases with the crack size. Figure 10 shows the maximum strain during crack propagation for each tested lever length (c). The metal yielding point imposes a limitation for the analysis of the test results.

The analytical SERR was calculated from test propagation points in the region of linear elastic propagation. Figure 11 shows the analytical and numerical fracture energy (G) of each tested lever length. The analytical curves were obtained using the global method (Eqs. 8 and 9) and the proposed method (Eqs. 13 and 14). The numerical curves were obtained from the finite elements model using the VCCT. Since the proposed method is reduced to the global method if a strain-based geometry is adopted for the MMB specimens, i.e., $\beta = 1$, as it is the case in this study, both analytical methods give very similar values of the mode I and mode II fracture energy. Consequently, the total fracture energy and mode partitioning are similar in both cases. When comparing analytical and numerical SERR, it is observed that the analytical SERR increases as the crack propagates while the numerical SERR remains in a narrow range. There is a considerable difference between analytical and numerical results in the first propagation point (30 mm) and the difference reduces as the crack propagates. However, the SERRs become similar when the crack length reaches 60 to 65 mm – see Figure 11a, 11b, 11c. This can be explained by the fact that the analytical methods take only into account the deformation due to bending when determining the energy, and neglect the deformation due to shear. The latter is significant when testing thick beams and becomes smaller as the thickness to span ratio decreases. Looking to the tested specimens, in the early stages of propagation, the thickness to crack length ratio is significantly higher than at further propagation stages when the crack length increases. Therefore, the deformation due to shear decreases as the crack increases, hence the analytical results get closer to the numerical ones.

The analytical and numerical fracture mode partitioning (G_I/G and G_{II}/G) are shown in Figure 12. It is important to notice that in all tested cases, the difference between the

partitioning ratio obtained with analytical and numerical models is limited to approximately 10%. Even though the proposed method did not give good predictions of the absolute values of the fracture energy, it gave relatively good predictions for the fracture mode partitioning. Therefore, the analytical methods should only be used to determine the mode partitioning but are limited in predicting the absolute values of fracture energy. The values of fracture energy and mode partitioning for each test showed in Figures 11 and 12 are presented in Appendix A.

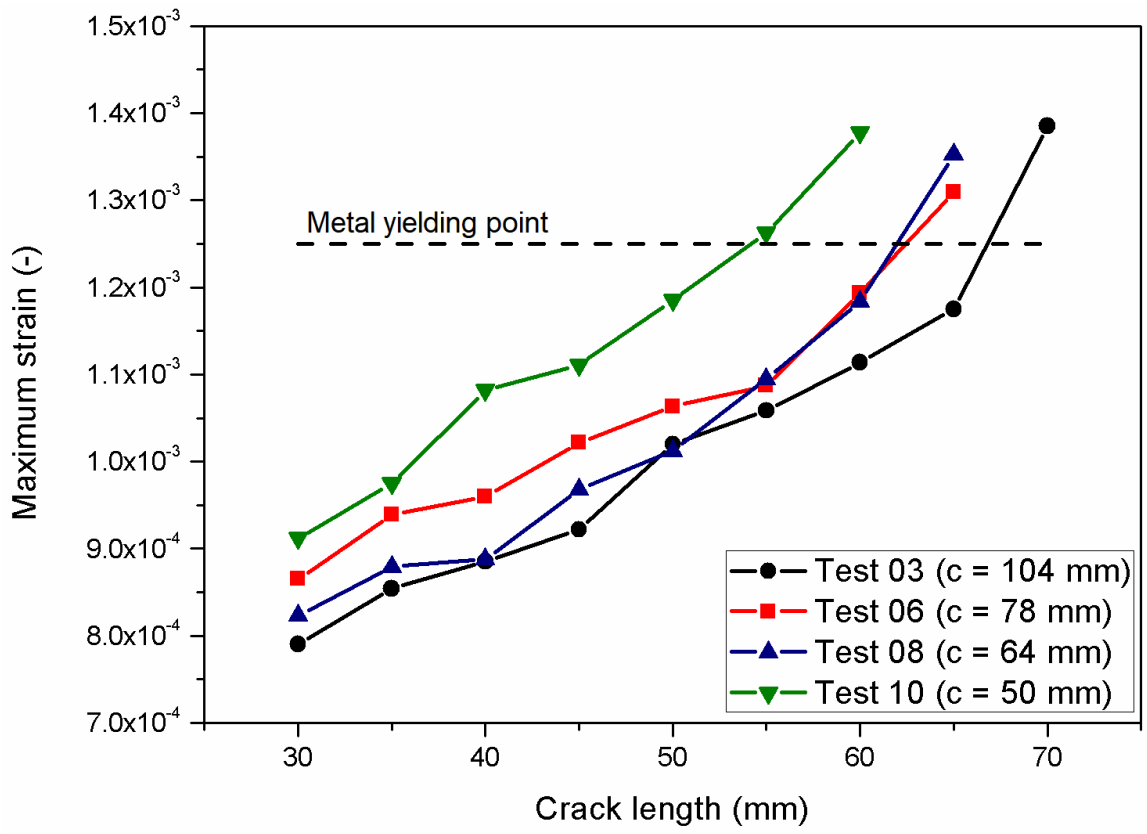

Figure 10: Maximum steel arm strain during crack propagation.

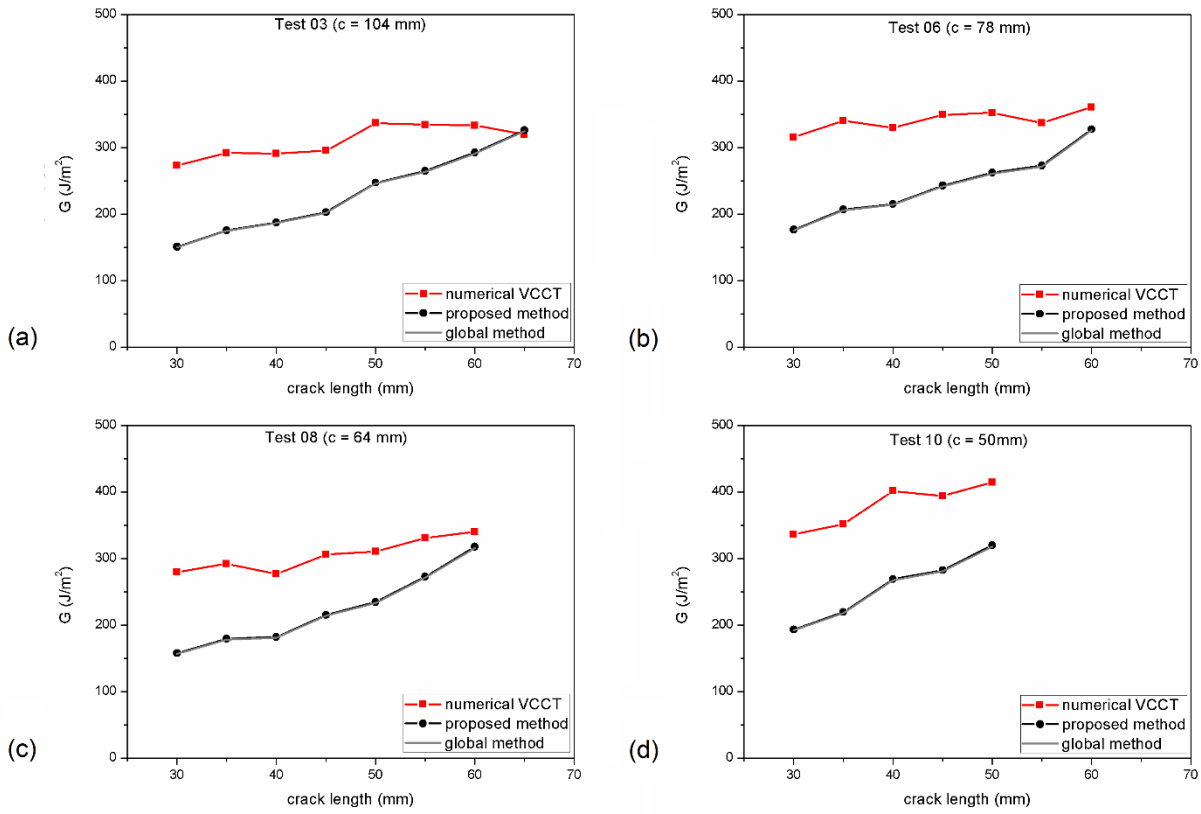

Figure 11: Analytical and numerical fracture energy of (a) Test 03, (b) Test 06, (c) Test 08 and (d) Test 10.

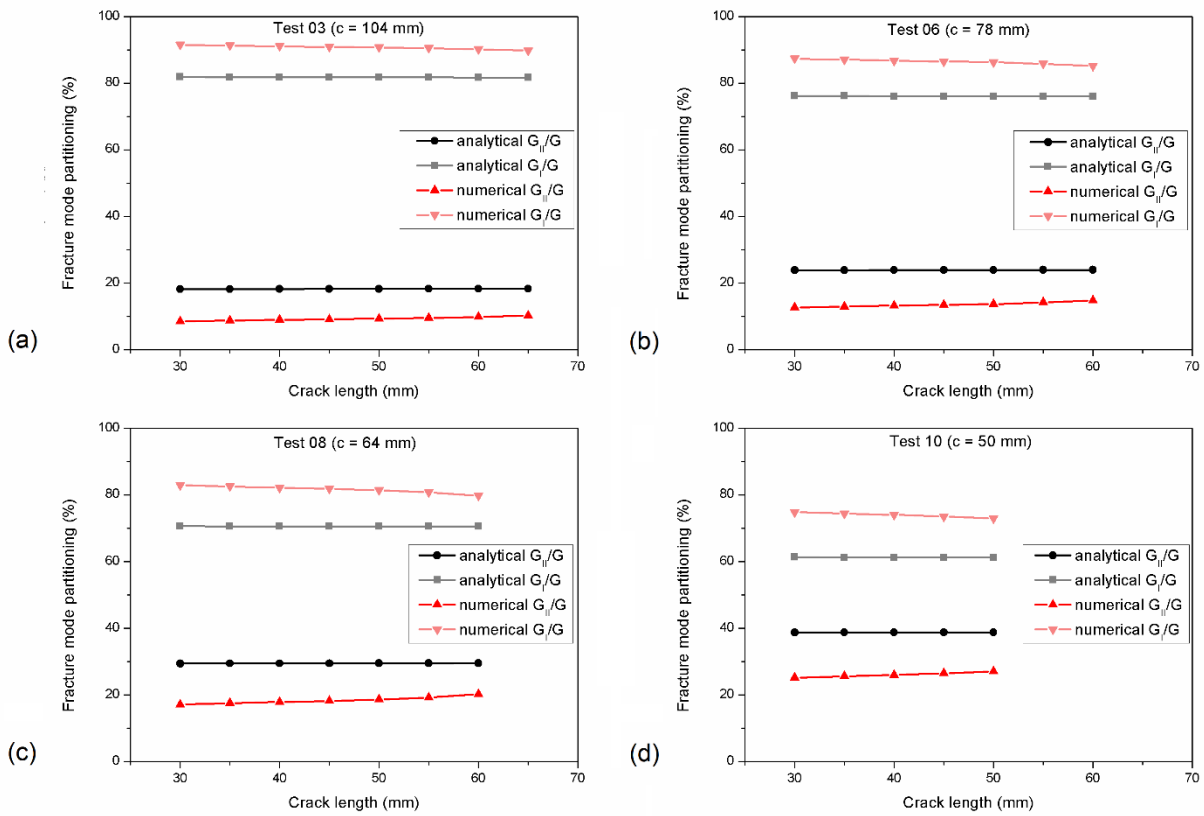

Figure 12: Analytical and numerical fracture mode partitioning of (a) Test 03, (b) Test 06, (c) Test 08 and (d) Test 10.

6. Conclusions

The mixed-mode fracture behaviour of a composite-to-metal adhesively bonded joint was investigated. A new strain-based criterion for the design of the Mixed-Mode Bending (MMB) bi-material specimen was suggested. A new analytical partitioning method was proposed and tested on a composite-to-metal bonded joint. A finite element model of the tests was developed and validated with strain gauges. The fracture energy was obtained from the numerical model using the VCCT. Analytical and numerical results were compared. The following conclusions can be drawn:

- The MMB test showed potential for testing mixed-mode fracture of bi-material bonded joints. The new strain-based specimen design was successfully applied to the MMB test;

- The metal yielding point imposes limitations on the maximum contribution of mode II fracture in the MMB test;
- The analytical model successfully predicts the fracture mode partitioning of bi-material bonded joints. However, it does not predict the absolute values of the SERR with accuracy, if the shear deformation is significant in the test;
- A finite elements model of the MMB test using the VCCT with a bi-material joint produces mesh size dependent results. Even though the crack propagates between elements with same material, the fracture mode partitioning showed some dependency on the element size. There is still a need for improvement in the prediction of fracture behavior of bi-material cracks using the VCCT.

Funding

This study was financed in part by the Coordenação de Aperfeiçoamento de Pessoal de Nível Superior - Brasil (CAPES); Conselho Nacional de Desenvolvimento Científico e Tecnológico (CNPq); Fundação Carlos Chagas Filho de Amparo à Pesquisa do Estado do Rio de Janeiro (FAPERJ); and the Netherlands Organisation for Scientific Research [project number 14366].

References

[1] Mangalgiri, P.D. Composite materials for aerospace applications. Bull. Mater. Sci. 1999, 22, 657–664. DOI: 10.1007/BF02749982.

[2] Taub, A.I.; Krajewski, P.E.; Luo, A.A. The evolution of technology for materials processing over the last 50 years: the automotive example. JOM 2007, 59, 48–57. DOI: 10.1007/S11837-007-0022-7.

[3] de Barros, S.; Banea, M.D.; Budhe, S. Experimental analysis of metal-composite repair of floating offshore units (FPSO). J. Adhes. 2016, 93, 147–158. DOI: 10.1080/00218464.2016.1177514.

[4] Van Den Einde, L.; Zhao, L.; Seible, F. Use of FRP composites in civil structural applications. Constr. Build. Mater. 2003, 17, 389–403. DOI: 10.1016/S0950-0618(03)00040-0.

[5] Budhe, S.; Banea, M.D.; de Barros, S. An updated review of adhesively bonded joints in composite materials. Int. J. Adhes. Adhes. 2017, 72, 30–42. DOI: 10.1016/j.ijadhadh.2016.10.010.

[6] Teixeira de Freitas, S.; Sinke, J. Failure analysis of adhesively-bonded skin-to-stiffener joints: Metal–metal vs. composite–metal. Eng. Failure Anal. 2015, 56, 2–13. DOI: 10.1016/j.engfailanal.2015.05.023.

[7] Teixeira de Freitas, S.; Sinke, J. Failure analysis of adhesively-bonded metal-skin-to-composite-stiffener: Effect of temperature and cyclic loading. Compos. Struct. 2017, 166, 27–37. DOI: 10.1016/j.compstruct.2017.01.027.

[8] Teixeira de Freitas, S.; Sinke, J. Adhesion Properties of Bonded Composite-to-Aluminium Joints Using Peel Tests. J. Adhes. 2014, 90, 511–525. DOI: 10.1080/00218464.2013.850424.

[9] Chaves, F.J.P.; da Silva, L.F.M.; de Moura, M.F.S.F.; Dillard, D.A.; Esteves, V.H.C. Fracture Mechanics Tests in Adhesively Bonded Joints - A Literature Review. J. Adhes. 2014, 90, 955–992. DOI: 10.1080/00218464.2013.859075.

[10] Lai, Y.-H.; Rakestraw, M.D.; Dillard, D.A. The cracked lap shear specimen revisited—a closed form solution. Int. J. Solids Struct. 1996, 33, 1725–1743. DOI: 10.1016/0020-7683(95)00124-7.

[11] Xiao, F.; Hui, C.-Y.; Kramer, E. J. Analysis of a mixed mode fracture specimen: the asymmetric double cantilever beam. J. Mater. Sci. 1993, 28, 5620–5629. DOI: 10.1007/BF00367838.

[12] Davidson, B.D.; Sundararaman V. A single leg bending test for interfacial fracture toughness determination. Int. J. Fract. 1996, 78, 193–210. DOI: 10.1007/BF00034525.

[13] Park, S; Dillard, D.A. Development of a simple mixed-mode fracture test and the resulting fracture energy envelope for an adhesive bond. Int. J. Fract. 2007, 148, 261–271. DOI: 10.1007/s10704-008-9200-z.

[14] Sørensen, B.F.; Jørgensen, K.; Jacobsen, T.K.; Østergaard, R.C. DCB-specimen loaded with uneven bending moments. Int. J. Fract. 2006, 141, 163–176. DOI: 10.1007/s10704-006-0071-x.

[15] Boyano, A.; Mollón, V.; Bonhomme, J.; de Gracia, J.; Arrese, A.; Mujika F. Analytical and numerical approach of an End Notched Flexure test configuration with an inserted roller for promoting mixed mode I/II. Eng. Fract. Mech. 2015, 143, 63–79. DOI: 10.1016/j.engfracmech.2015.06.031.

[16] Fernlund, G.; Spelt, J.K. Mixed-mode fracture characterization of adhesive joints. Compos. Sci. Technol. 1994, 50, 441–449. DOI: 10.1016/0266-3538(94)90052-3.

[17] Reeder, J.R.; Crews Jr, J.H. Mixed-Mode bending method for delamination testing. AIAA J. 1990, 27, 1270–1276. DOI: 10.2514/3.25204.

[18] Costa, M.; Carbas, R.; Marques, E.; Viana, G.; da Silva, L.F.M. An apparatus for mixed-mode fracture characterization of adhesive joints. Theor. Appl. Fract. Mech. 2017, 91, 94–102. DOI: 10.1016/j.tafmec.2017.04.014.

[19] Reeder, J.R.; Crews Jr., J.H. Redesign of the Mixed-mode Bending Delamination Test to Reduce Non-linear Effects. J. Compos. Technol. Res. 1992, 14, 12–19. DOI: 10.1520/CTR10078J.

[20] Ducept, F.; Gamby, D.; Davies, P. A mixed-mode failure criterion derived from tests on symmetric and asymmetric specimens. Compos. Sci. Technol. 1999, 59, 609–619. DOI: 10.1016/S0266-3538(98)00105-5.

[21] Pereira, A.B; de Morais, A.B. Mixed mode I + II interlaminar fracture of glass-epoxy multidirectional laminates – Part 2 Experiments. Compos. Sci. Technol. 2006, 66, 1896–1902. DOI: 10.1016/j.compscitech.2006.04.008.

[22] Kim, B.W.; Mayer, A.H. Influence of fiber direction and mixed-mode ratio on delamination fracture toughness of carbon/epoxy laminates. Compos. Sci. Technol. 2003, 63, 695–713. DOI: 10.1016/S0266-3538(02)00258-0.

[23] Pereira, A.B.; de Morais, A.B. Mixed mode I + II interlaminar fracture of carbon/epoxy laminates. Composites, Part A 2008, 39, 322–333. DOI: 10.1016/j.compositesa.2007.10.013.

[24] Shahverdi, M.; Vassilopoulos, A.P.; Keller, T. Mixed-Mode I/II fracture behavior of asymmetric adhesively-bonded pultruded composite joints. Eng. Fract. Mech. 2014, 115, 43–59. DOI: 10.1016/j.engfracmech.2013.11.014.

[25] Liu, Z.; Gibson, R.F.; Newaz, G.M. The Use of a Modified Mixed Mode Bending Test for Characterization of Mixed-Mode Fracture Behavior of Adhesively Bonded Metal Joints. J. Adhes. 2010, 78, 223–244. DOI: 10.1080/00218460210408.

[26] Stamoulis, G.; Carrere, N.; Cognard, J.Y.; Davies, P.; Badulescu, C. On the experimental mixed-mode failure of adhesively bonded metallic joints. Int. J. Adhes. Adhes. 2014, 51, 148–158. DOI: 10.1016/j.ijadhadh.2014.03.002.

[27] Droubi, M.G.; Mcafee, J.; Horne, R.C.; Walker, S.; Klaassen, C.; Crawford, A.; Prathuru, A.K.; Faisal, N.H. Mixed-mode fracture characteristics of metal-to-metal adhesively bonded joints - experimental and simulation methods. Procedia Structural Integrity 2016, 5, 40–47. DOI: 10.1016/j.prostr.2017.07.059.

[28] Oliveira, J.M.Q.; de Moura, M.F.S.F.; Silva, M.A.L.; Morais J.J.L. Numerical analysis of the MMB test for mixed-mode I/II wood fracture. Compos. Sci. Technol. 2007, 67, 1764–1771. DOI: 10.1016/j.compscitech.2006.11.007.

[29] de Moura, M.F.S.F.; Oliveira, J.M.Q.; Morais J.J.L; Dourado N. Mixed-mode (I + II) fracture characterization of wood bonded joints. Constr. Build. Mater. 2011, 25, 1956–1962. DOI: 10.1016/j.conbuildmat.2010.11.060.

[30] Yoshihara, H. Initiation and propagation fracture toughness of solid wood under the mixed Mode I-II condition examined by mixed-mode bending test. Eng. Fract. Mech. 2013, 104, 1–15. DOI: 10.1016/j.engfracmech.2013.03.023.

[31] Pereira, F.A.M.; de Moura, M.F.S.F.; Dourado, N.; Morais, J.J.L.; Silva, F.G.A.; Dias, M.I.R. Bone fracture characterization under mixed-mode I + II loading using the MMB test. Eng. Fract. Mech. 2016, 166, 151–163. DOI: 10.1016/j.engfracmech.2016.08.011.

[32] Luis Távara, L.; Reinoso, J.; Castillo, D.; Mantič, V. Mixed-mode failure of interfaces studied by the 2D linear elastic–brittle interface model: Macro- and micro-mechanical finite-element applications in composites. J. Adhes. 2018, 94, 627–656. DOI: 10.1080/00218464.2017.1320988.

[33] Krueger, R. Virtual crack closure technique: History, approach, and applications. Appl. Mech. Rev. 2004, 57, 109–143. DOI: 10.1115/1.1595677.

[34] Agrawal, A.; Karlsson, A.M. Obtaining mode mixity for a bimaterial interface crack using the virtual crack closure technique. Int. J. Fract. 2006, 141, 75–98. DOI: 10.1007/s10704-006-0069-4.

[35] Williams, J.G. On the calculation of energy release rates for cracked laminates. Int. J. Fract. 1988, 36, 101–119. DOI: 10.1007/BF00017790.

[36] Hibbeler, R. C. Mechanics of Materials, seventh edition; Pearson Prentice Hall: São Paulo, 2010.

[37] Harvey, C.M.; Wang, S. Experimental assessment of mixed-mode partition theories. Compos. Struct. 2012, 94, 2057–2067. DOI: 10.1016/j.compstruct.2012.02.007.

[38] Wang, W.; Fernandes, R.L.; Teixeira de Freitas, S.; Zarouchas, D. How pure mode I can be obtained in bi-material bonded DCB joints: A longitudinal strain-based criterion. Composites, Part B 2018, 153, 137–148. DOI: 10.1016/j.compositesb.2018.07.033.

[39] Teixeira de Freitas, S.; Banea, M.D.; Budhe, S.; de Barros, S. Interface adhesion assessment of composite-to-metal bonded joints under salt spray conditions using peel tests. Compos. Struct. 2017, 164, 68–75. DOI: 10.1016/j.compstruct.2016.12.058.

[40] Meniconi.,L.C.M.; Porciúncula, I.N.; McGeorge;,D.; Pedersen, A. Structural repair at a production platform by means of a composite material patch. Presented at the Offshore Technology Conference, Houston, Texas, USA, May 3-6, 2010.

[41] ASTM International, D6671M-13: Standard Test Method for Mixed Mode I-Mode II Interlaminar Fracture Toughness of Unidirectional Fiber Reinforced Polymer Matrix Composites, http://www.astm.org/cgi-bin/resolver.cgi?D6671D6671M-13e1 (accessed Feb 22, 2018).

Appendix A

Analytical and numerical fracture energy of Test 03, Test 06, Test 08 and Test 10.

Table A1: Test 03 fracture energy.

Crack length, a (mm)	G_I (J/m^2)		G_{II} (J/m^2)		G (J/m^2)		G_{II}/G (%)		G_I/G (%)	
	Anal.	Num.	Anal.	Num.	Anal.	Num.	Anal.	Num.	Anal.	Num.
30	123.3	249.7	27.4	23.2	150.7	272.9	18.2	8.5	81.8	91.5
35	143.5	266.4	31.9	25.5	175.4	291.9	18.2	8.7	81.8	91.3

40	153.2	264.7	34.2	26.0	187.3	290.7	18.2	8.9	81.8	91.1
45	165.8	268.4	37.0	27.0	202.8	295.4	18.3	9.1	81.7	90.9
50	201.9	305.6	45.1	31.3	247.0	336.8	18.3	9.3	81.7	90.7
55	216.4	302.6	48.4	31.8	264.8	334.4	18.3	9.5	81.7	90.5
60	239.1	300.5	53.5	32.7	292.6	333.3	18.3	9.8	81.7	90.2
65	266.4	286.9	59.7	32.7	326.1	319.6	18.3	10.2	81.7	89.8

Table A2: Test 06 fracture energy.

Crack length, a (mm)	G_I (J/m^2)		G_{II} (J/m^2)		G (J/m^2)		G_{II}/G (%)		G_I/G (%)	
	Anal.	Num.	Anal.	Num.	Anal.	Num.	Anal.	Num.	Anal.	Num.
30	134.4	275.7	42.1	40.0	176.5	315.7	23.8	12.7	76.2	87.3
35	157.6	296.2	49.4	44.1	207.0	340.4	23.9	13.0	76.1	87.0
40	163.6	286.1	51.4	43.7	215.1	329.8	23.9	13.3	76.1	86.7
45	184.9	302.1	58.1	47.2	243.0	349.2	23.9	13.5	76.1	86.5
50	199.4	303.9	62.8	48.3	262.2	352.2	23.9	13.7	76.1	86.3
55	207.5	289.0	65.4	48.0	272.9	337.0	24.0	14.2	76.0	85.8
60	248.8	307.2	78.5	53.6	327.3	360.8	24.0	14.8	76.0	85.2

Table A3: Test 08 fracture energy.

Crack length, a (mm)	G_I (J/m^2)		G_{II} (J/m^2)		G (J/m^2)		G_{II}/G (%)		G_I/G (%)	
	Anal.	Num.	Anal.	Num.	Anal.	Num.	Anal.	Num.	Anal.	Num.
30	111.5	231.7	46.4	47.9	158.0	279.6	29.4	17.1	70.6	82.9
35	126.6	241.0	52.7	51.1	179.3	292.1	29.4	17.5	70.6	82.5

40	128.5	227.2	53.6	49.4	182.1	276.6	29.4	17.8	70.6	82.2
45	151.8	250.3	63.4	55.6	215.2	305.9	29.5	18.2	70.5	81.8
50	165.4	252.7	69.1	57.8	234.5	310.5	29.5	18.6	70.5	81.4
55	192.3	267.1	80.4	63.6	272.8	330.7	29.5	19.2	70.5	80.8
60	223.9	271.6	93.7	69.0	317.5	340.5	29.5	20.3	70.5	79.7

Table A4: Test 10 fracture energy.

Crack length, a (mm)	G_I (J/m^2)		G_{II} (J/m^2)		G (J/m^2)		G_{II}/G (%)		G_I/G (%)	
	Anal.	Num.	Anal.	Num.	Anal.	Num.	Anal.	Num.	Anal.	Num.
30	118.5	251.7	74.8	84.6	193.3	336.3	38.7	25.1	61.3	74.9
35	134.6	261.7	85.1	90.0	219.6	351.8	38.7	25.6	61.3	74.4
40	164.8	297.2	104.2	104.3	269.0	401.5	38.7	26.0	61.3	74.0
45	172.9	289.7	109.5	104.4	282.4	394.1	38.8	26.5	61.2	73.5
50	195.8	302.4	124.0	112.2	319.7	414.7	38.8	27.1	61.2	72.9